METABOLISM

# Large-scale functional analysis of the roles of phosphorylation in yeast metabolic pathways

Juliane Caroline Schulz,[1]* Mattia Zampieri,[1]* Stefanie Wanka,[2] Christian von Mering,[2] Uwe Sauer[1]†

**Protein phosphorylation is a widespread posttranslational modification that regulates almost all cellular functions. To investigate the large number of phosphorylation events with unknown functions, we monitored the concentrations of several hundred intracellular metabolites in *Saccharomyces cerevisiae* yeast strains with deletions of 118 kinases or phosphatases. Whereas most deletion strains had no detectable difference in growth compared to wild-type yeast, two-thirds of deletion strains had alterations in metabolic profiles. For about half of the kinases and phosphatases encoded by the deleted genes, we inferred specific regulatory roles on the basis of knowledge about the affected metabolic pathways. We demonstrated that the phosphatase Ppq1 was required for metal homeostasis. Combining metabolomic data with published phosphoproteomic data in a stoichiometric model enabled us to predict functions for phosphorylation in the regulation of 47 enzymes. Overall, we provided insights and testable predictions covering greater than twice the number of known phosphorylated enzymes in yeast, suggesting extensive phosphorylation-dependent regulation of yeast metabolism.**

## INTRODUCTION

Reversible protein phosphorylation is a key regulatory mechanism of many cellular functions in all living species (*1*, *2*). A complex hierarchical network of kinases and phosphatases, known as the kinome, regulates phosphorylation of about 30% of the human proteome and 75% of the yeast proteome (*3*, *4*). Signaling by the kinome affects proteins at multiple regulatory layers, controlling the activity, abundance, and localization of proteins (*5*).

The yeast *Saccharomyces cerevisiae* is extensively used as a model organism to investigate the functionality of phosphorylation events. Early studies in yeast were mostly aimed at identifying kinase substrates using in vitro kinase assays (*6*), whereas recent technological advances have enabled proteome-wide mapping of phosphorylation sites in vivo (*7*). Systems-level studies monitoring growth (*1*, *8*) or changes in the abundance of transcripts (*9*) or protein phosphorylation (*7*) in yeast have resolved the effect of deletion or overexpression of individual members of a network of greater than 130 kinases and 50 phosphatases. These studies provide an invaluable resource to investigate the global impact of phosphorylation on adaptation to environmental (*10*) or internal signals (*11*).

Here, we investigated the regulatory impact of phosphorylation in modulating not only central metabolic pathways, such as glycolysis or the tricarboxylic acid (TCA) cycle, but also peripheral metabolic pathways, such as amino acid and nucleotide synthesis and degradation. Although a relatively comprehensive topology of the yeast kinome network is emerging (*7*, *12*), methods capable of systematically assessing the in vivo relevance and function of protein phosphorylation lag behind. To investigate the impact of deletion of individual phosphatases or kinases on yeast metabolism, we used a nontargeted mass spectrometry (MS) approach (*13*) capable of quantifying about 28% of the metabolites in *S. cerevisiae* (*14*). We considered the concentration of metabolites as functional readouts that integrate effects from multiple regulatory mechanisms converging on metabolic enzyme activity. To assess the role of protein phosphorylation in the regulation of metabolism, we evaluated metabolic profiles of a library of 118 kinase and phosphatase yeast deletion strains grown in chemically defined medium identical to that previously used to grow these yeast deletion strains for phosphoproteomic analyses (*7*), and integrated our metabolomics data with the published phosphoproteomics data. By quantifying relative changes in the concentrations of hundreds of intracellular metabolites between wild-type yeast and yeast with individual kinase or phosphatase deletions, we expanded the range of observed phenotypes beyond those routinely monitored in classical physiological studies.

[1]Institute of Molecular Systems Biology, Eidgenössische Technische Hochschule (ETH) Zürich, 8093 Zürich, Switzerland. [2]Institute of Molecular Life Sciences and Swiss Institute of Bioinformatics, University of Zürich, 8057 Zürich, Switzerland.
*These authors contributed equally to this work.
†Corresponding author. E-mail: sauer@imsb.biol.ethz.ch

## RESULTS

### Metabolic profiles of yeast strains with deletions of genes encoding kinases or phosphatases

More than half of the 900 metabolic enzymes in yeast are phosphorylated, but the extent to which changes in the phosphorylation state of a metabolic enzyme modifies its activity in vivo is known for only 24 enzymes (table S1). To understand how alterations in protein phosphorylation affect the composition of metabolites in yeast, we performed metabolic profiling of mutant yeast using a recently developed nontargeted MS approach (*13*). We grew 118 yeast strains with deletions of genes encoding 91 kinases and 27 phosphatases in sextuplet in 96-well plates in synthetic defined medium with glucose and amino acids. In these conditions, fewer than 10% of the yeast deletion strains had growth rates that deviated greater than 20% from that of wild-type yeast (fig. S1). We extracted intracellular metabolites during the exponential growth phase and analyzed the concentrations of metabolites using direct injection and time-of-flight (TOF) MS (*13*). In total, we detected 1710 ions that we annotated with putative identities using metabolite masses from the Kyoto Encyclopedia of Genes and Genomes (KEGG) database (*15*) (table S2). When we considered only metabolites annotated within the genome-wide metabolic model of yeast (*14*), 145 observed ions matched 216 deprotonated annotated metabolites, whereas when we included ions with neutral losses (table S2), 500 observed ions matched 716 deprotonated annotated metabolites.

To identify changes in the concentrations of metabolites induced by inactivation of kinases or phosphatases, we calculated the ion intensity

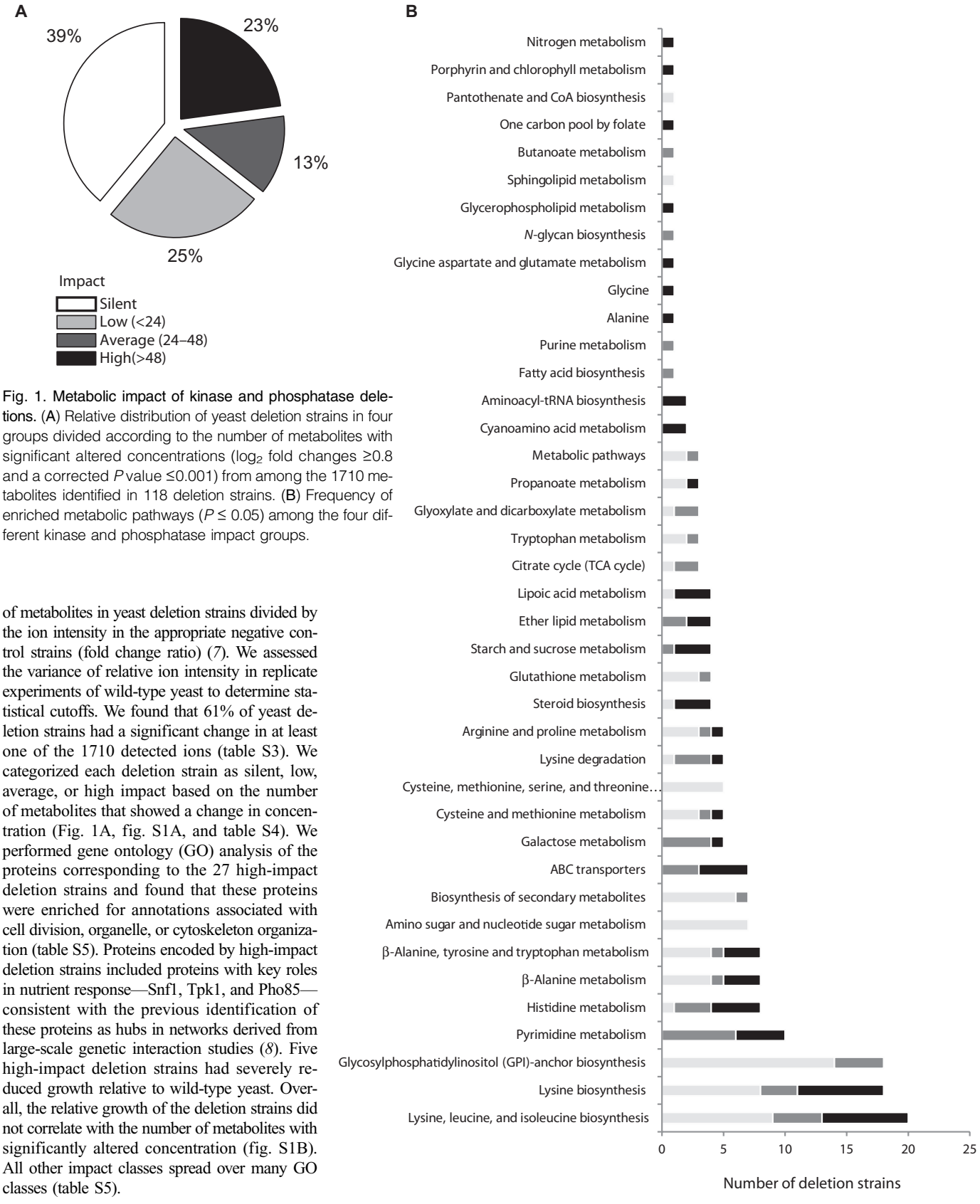


Fig. 1. Metabolic impact of kinase and phosphatase deletions. (A) Relative distribution of yeast deletion strains in four groups divided according to the number of metabolites with significant altered concentrations ($log_2$ fold changes ≥0.8 and a corrected *P* value ≤0.001) from among the 1710 metabolites identified in 118 deletion strains. (B) Frequency of enriched metabolic pathways ($P \leq 0.05$) among the four different kinase and phosphatase impact groups.

of metabolites in yeast deletion strains divided by the ion intensity in the appropriate negative control strains (fold change ratio) (*7*). We assessed the variance of relative ion intensity in replicate experiments of wild-type yeast to determine statistical cutoffs. We found that 61% of yeast deletion strains had a significant change in at least one of the 1710 detected ions (table S3). We categorized each deletion strain as silent, low, average, or high impact based on the number of metabolites that showed a change in concentration (Fig. 1A, fig. S1A, and table S4). We performed gene ontology (GO) analysis of the proteins corresponding to the 27 high-impact deletion strains and found that these proteins were enriched for annotations associated with cell division, organelle, or cytoskeleton organization (table S5). Proteins encoded by high-impact deletion strains included proteins with key roles in nutrient response—Snf1, Tpk1, and Pho85—consistent with the previous identification of these proteins as hubs in networks derived from large-scale genetic interaction studies (*8*). Five high-impact deletion strains had severely reduced growth relative to wild-type yeast. Overall, the relative growth of the deletion strains did not correlate with the number of metabolites with significantly altered concentration (fig. S1B). All other impact classes spread over many GO classes (table S5).

Phosphorylation-mediated metabolic changes may be induced by modulation of enzyme activity or by alterations in local protein abundance due to degradation, translocation, or transcription. However, significant transcriptional changes are present in only 26% of these kinase and phosphatase deletion strains (*9*), which is comparable to the low percentage (10%) of strains we observed with obvious growth phenotypes (table S4), but contrasts the large percentage (78%) of strains with significant changes in protein phosphorylation (*7*). Thus, direct effects due to the deletion of kinases and phosphatases may be more frequent than indirect effects on transcription mediated by changes in the activity of transcription factors, suggesting that steady-state metabolic changes in these deletion strains are more likely to result from modulation of phosphorylation rather than transcription of metabolic enzymes.

To test if the deletion of kinases or phosphatases that perform related functions led to similar patterns of metabolic changes, we calculated the pairwise similarity between metabolic profiles of each deletion strain and clustered the strains using an affinity propagation algorithm (*16*) into 15 different groups (table S4). Several clusters were enriched for at least one GO category or for "functional" interactions according to the STRING database (*17*) (table S6). Most of the phosphatases or kinases involved in global processes, such as cell cycle or mating, clustered together. For example, Pph20 and Pph21—two alternative catalytic subunits of protein phosphatase 2A (PP2A) (*18*)—clustered together, whereas Ptc4 and Sdp1—two phosphatases that interact with the mitogen-activated protein (MAP) kinase SLT2 (*17*)—clustered together (table S4). In contrast, we observed divergent metabolic profiles for some proteins that regulate analogous metabolic functions—for example, among Tpk1, Tpk2, and Tpk3, which are different isoforms of the catalytic unit of protein kinase A (PKA) (*19*), suggesting that these proteins may have nonredundant roles. In addition, divergence of metabolic profiles in yeast with deletion of genes encoding related proteins could result from condition-dependent activity. For example, Ptc6 and Ptc5 are phosphatases that dephosphorylate and thereby inactivate pyruvate dehydrogenase (*20*). However, only Ptc6, and not Ptc5, showed significant metabolic changes (table S3), suggesting that only Ptc6 is active in the chemically defined medium used in this study.

One of the largest clusters of deletion strains with similar metabolic profiles contained 11 kinases (cluster number 100; table S4). Most of these kinases had functional or physical interactions with each other as annotated in STRING (table S6). Moreover, most of these kinases are involved in responses to stress (*21*, *22*). Two kinases in this cluster, STE11 and FUS3, are involved in pheromone signaling (*23*). α-Trehalose plays a role in stress responses and desensitization to stimulation with the pheromone α factor (*24*), and α-trehalose accumulated in all deletion strains in this cluster (Fig. 2A and table S4). Three of the proteins in this cluster—AKL1, SKM1, and VHS1—have no known interaction (annotated in the STRING database) with the other eight proteins in the cluster (Fig. 2B). Thus, we identified clusters of kinases and phosphatases that are required for complex metabolic regulation in yeast that largely occurs independent of transcriptional regulation and growth.

## Reconstruction of metabolic associations for kinases and phosphatases

To gain a system-level understanding of how kinases and phosphatases regulate various metabolic enzymes, we performed an enrichment analysis of the KEGG pathway annotations for metabolites that were altered in kinase and phosphatase deletion strains. For about 80% of the kinase and phosphatase deletion strains with detectable metabolic changes, we found at least one significantly enriched pathway (table S7). Generally, the affected metabolites were not evenly distributed over the metabolic network but were frequently components of peripheral metabolic pathways. For example, many deletion strains had changes in metabolites associated with metabolism of lysine, glycosylphosphatidylinositol, pyrimidine, histidine, or β-alanine (Fig. 1B) (table S7). The low complexity of the metabolic responses in the low-impact deletion strains enabled us to identify previously unknown relationships between six kinases or phosphatases and the metabolism of pantothenate, sphingolipid, propanoate or tryptophan, or the TCA cycle (Fig. 1B). In most high-impact deletion strains, affected metabolites clustered in four or fewer metabolic pathways (fig. S2). For example, the affected metabolites in the high-impact deletion strain corresponding to the kinase Snf1 were only enriched in the glycolysis and glycerolphospholipid synthesis pathways (table S7), consistent with the role of Snf1 in regulating glycolysis and lipid biosynthesis (*25*).

Although many phosphorylated enzymes affect the TCA cycle (*26*), only the *oca1*Δ, *ptc6*Δ, and *ppq1*Δ strains had metabolic profiles enriched for this pathway (table S7). Of these three, only PTC6 is reported to influence cellular respiration (*20*). *PPQ1* and *OCA1* show a strong positive genetic interaction (*8*). However, the proteins encoded by these genes have

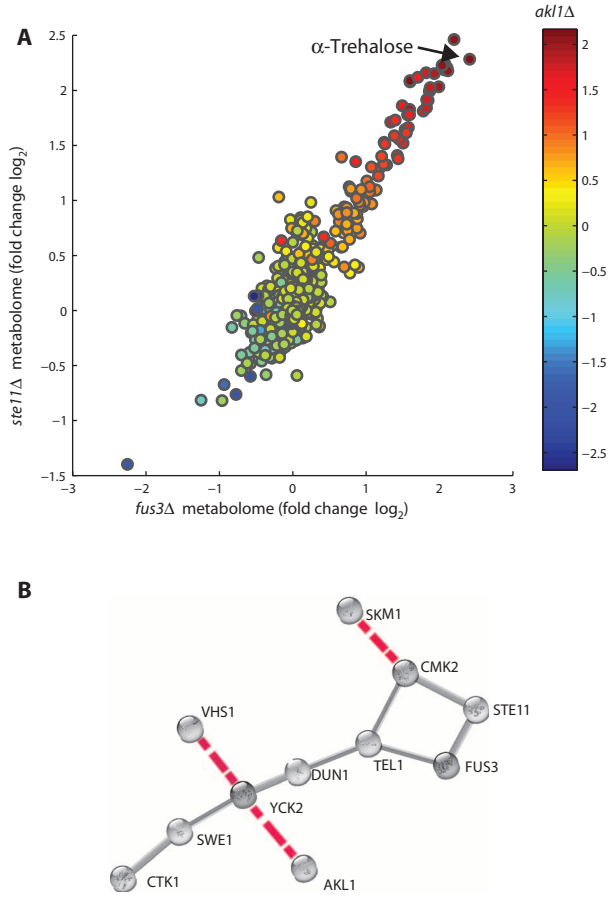


Fig. 2. Deletions of kinases and phosphatases eliciting similar metabolic profiles. (**A**) Scatter plot comparing metabolic changes ($log_2$ fold changes) observed in *fus3*Δ and *ste11*Δ (Pearson correlation coefficient = 0.89). Dots are color-coded according to the magnitude of changes observed in a third deletion strain (*akl1*Δ) (Pearson correlation coefficient = 0.82). (**B**) Network graph of interactions among proteins annotated in the STRING database (*17*) corresponding to deletion strains in the same metabolome-based cluster (cluster 100 in table S4). Red dashed lines indicate that there was no interaction in STRING.

divergent functions. PPQ1 regulates translational accuracy (*27*), whereas *OCA1* is required for cell cycle arrest in response to oxidative damage (*28*). Deletion of *OCA1* caused metabolic changes in several pathways, whereas deletion of *PPQ1* specifically affected the TCA cycle metabolites citrate and isocitrate, which exhibited the largest increases in *ppq1*Δ yeast (table S3). Targeted liquid chromatography–tandem MS (LC-MS/MS) showed that the concentration of citrate was equally increased in the auxotrophic and prototrophic deletion strains of *PPQ1*, but that there was less accumulation of the downstream metabolite isocitrate in the prototrophic deletion strain of *PPQ1* (Fig. 3A).

To understand the relationship between Ppq1 and the TCA cycle, we evaluated metabolic profiles of *ppq1*Δ yeast in different nutrient conditions. Citrate is the first intermediate in the oxidative branch of the TCA cycle, and the increased abundance of citrate in *ppq1*Δ yeast could reflect imbalanced cellular respiration. *ppq1*Δ yeast had higher citrate concentrations when grown with the carbon sources ethanol or galactose, which are substrates that favor oxidative metabolism (*29*), compared to glucose, which promotes fermentative (glycolytic) metabolism (Fig. 3B). The rate of exponential growth of *ppq1*Δ yeast was similar to the wild-type yeast when grown on most carbon sources and slightly slower on ethanol (table S8).

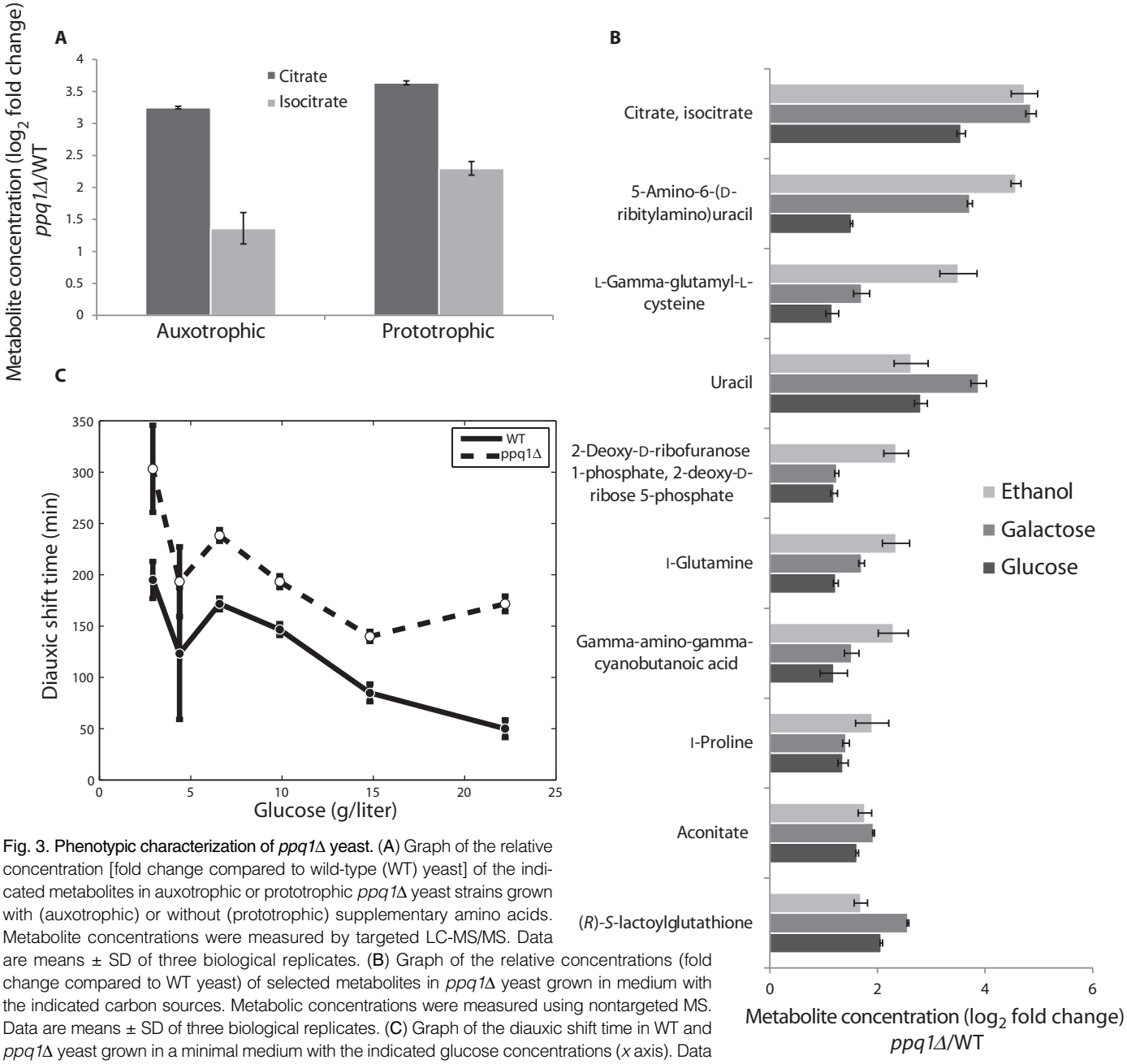


Fig. 3. Phenotypic characterization of *ppq1*Δ yeast. (A) Graph of the relative concentration [fold change compared to wild-type (WT) yeast] of the indicated metabolites in auxotrophic or prototrophic *ppq1*Δ yeast strains grown with (auxotrophic) or without (prototrophic) supplementary amino acids. Metabolite concentrations were measured by targeted LC-MS/MS. Data are means ± SD of three biological replicates. (B) Graph of the relative concentrations (fold change compared to WT yeast) of selected metabolites in *ppq1*Δ yeast grown in medium with the indicated carbon sources. Metabolic concentrations were measured using nontargeted MS. Data are means ± SD of three biological replicates. (C) Graph of the diauxic shift time in WT and *ppq1*Δ yeast grown in a minimal medium with the indicated glucose concentrations (*x* axis). Data are means ± SD of three biological replicates. $P < 0.01$ for all concentrations of glucose, paired *t* test.

However, the diauxic shift from glucose to ethanol was greatly delayed in *ppq1*Δ yeast compared to wild-type yeast (Fig. 3C), suggesting that Ppq1 is important for adaptation on nonfermentable carbon sources.

To investigate the mechanism by which Ppq1 affects the TCA cycle–related processes, we explored the functions of proteins that are differentially phosphorylated in *ppq1*Δ yeast compared to wild-type yeast. Among 24 proteins that are differentially phosphorylated in *ppq1*Δ yeast, Spl2 and Pho84 are the proteins with the largest increase in phosphorylation (table S9) (*7*). Spl2 decreases low-affinity phosphate transport in yeast grown in medium with reduced phosphates (*30*), and *pho84*Δ yeast have enhanced resistance to high concentrations of manganese (Mn) (*31*). The largest reduction in phosphorylation of any protein in *ppq1*Δ yeast occurs on the cytosolic superoxide dismutase Sod1 (*7*). Growth defects in *sod1*Δ yeast are reversed by supplementing the growth medium with Mn, which generates catalytic Mn antioxidants that can directly react with superoxide and protect proteins from oxidative damage providing an intracellular ROS (reactive oxygen species) scavenging activity (*32*, *33*). Moreover, the cellular redox state directly affects the activity of several enzymes in the TCA cycle (*34*–*36*), and deletion of the Mn-binding mitochondrial superoxide dismutase (Sod2) increases the concentration of citrate by impairing Aco1, the enzyme that converts citrate to isocitrate through an aconitate intermediate (*36*). Thus, the associated differential phosphorylation of Pho84 and Sod1 and increased concentration of citrate suggested the existence of regulatory mechanisms that compensate for an imbalance of Mn or redox homeostasis in *ppq1*Δ yeast.

To test if Ppq1 was required for Mn homeostasis and the oxidative stress response, we monitored changes in metabolic profiles of wild-type and *ppq1*Δ yeast exposed to excess Mn or the oxidative stress–inducing agent paraquat. The metabolic profiles (Fig. 4A) and inhibition of growth (Fig. 4B) induced by paraquat were almost indistinguishable between *ppq1*Δ and wild-type yeast. However, in the presence of excess Mn, *ppq1*Δ yeast had a different metabolic response (Fig. 4A) and were more

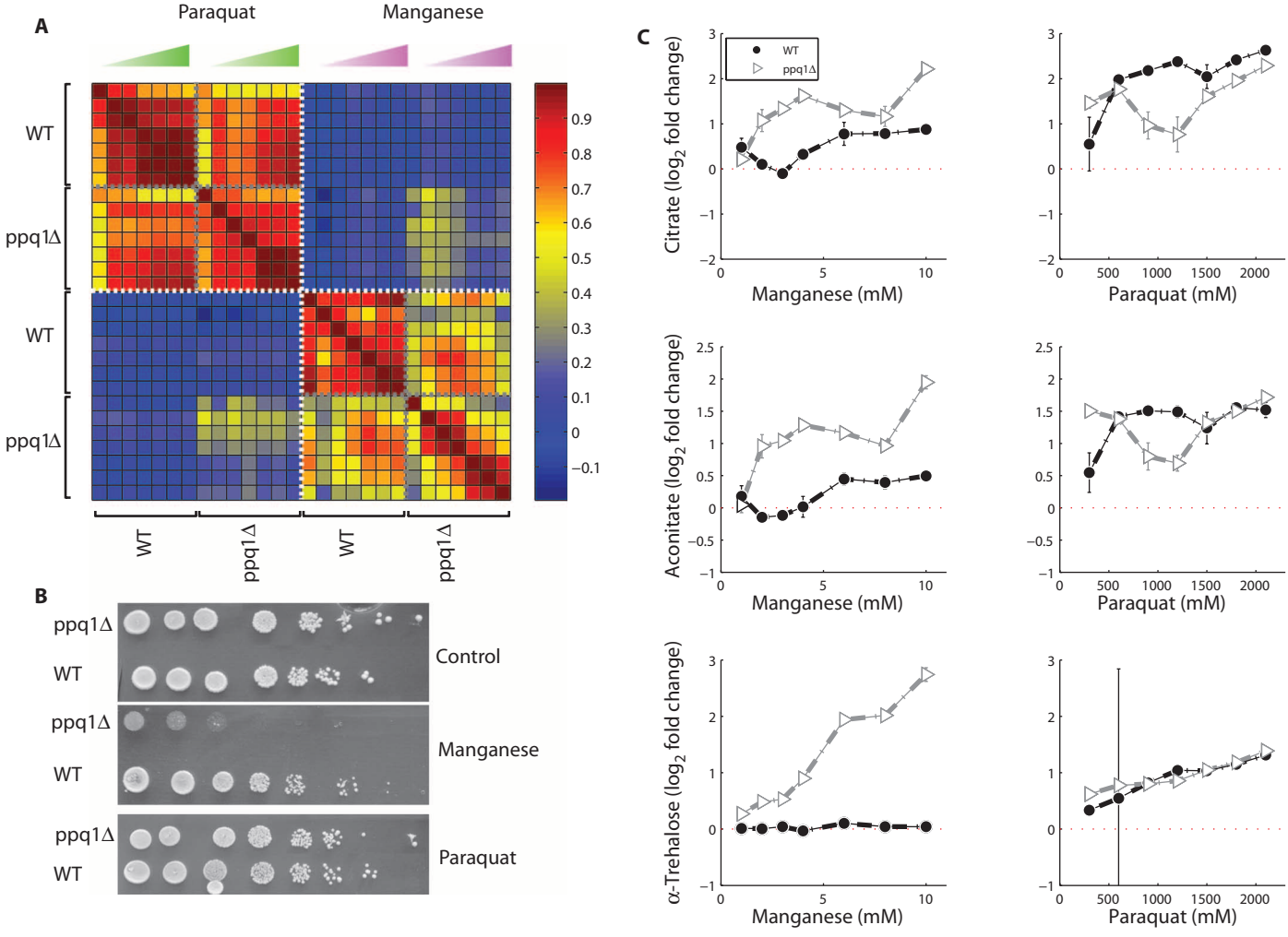


Fig. 4. Metabolomic response of *ppq1*Δ yeast to environmental stress. (A) Symmetric heatmap of pairwise Pearson similarity between the metabolomic responses to excess Mn or paraquat in WT or *ppq1*Δ yeast. (B) Spot assay of sensitivity to growth inhibition by excess Mn or paraquat. A series of fivefold dilutions of exponentially growing *ppq1*Δ and WT yeast were spotted on agar plates containing galactose as carbon source and either MnCl (4 mM) or paraquat (250 μM). A representative example of triplicate experiments is shown. (C) Fold changes of citrate, aconitate, and α-trehalose concentrations before and after 2 hours of exposure to excess Mn or paraquat. Data are means ± SD of three biological replicates.

sensitive to growth inhibition (Fig. 4B) compared to wild-type yeast. Moreover, in wild-type yeast, the concentrations of citrate and aconitate were more sensitive to excess Mn than other metabolites, including the stress-responsive metabolite α-trehalose. There was a larger increase in citrate and aconitate in response to excess Mn in *ppq1*Δ yeast compared to wild-type yeast (Fig. 4, A and C), consistent with the hypothesis that *ppq1*Δ yeast have an impaired response to excess Mn, primarily reflected in an altered concentration of the early intermediates in the oxidative branch of the TCA cycle. Exposure to paraquat increased the concentration of α-trehalose in both wild-type and *ppq1*Δ yeast (Fig. 4C). In contrast, exposure to excess Mn increased the concentration of α-trehalose in *ppq1*Δ, but not in wild-type yeast (Fig. 4C). Therefore, Ppq1 suppresses the activity of proteins that govern Mn homeostasis and thereby affects the activity of the TCA cycle.

## Inferring functionality of phosphorylation events

The similarity of metabolic profiles among different kinase and phosphatase yeast deletion strains (table S4) suggested that there may be functional similarities among the encoded proteins. Therefore, we derived a map of interactions between kinases and phosphatases and the metabolic pathways enriched for metabolites that were differentially regulated in kinase or phosphatase deletion strains (Fig. 1 and table S7). To identify the function of individual phosphorylation events, we integrated published phosphoproteomics data (*7*) with our metabolomics data (fig. S6). We hypothesized that the largest changes in the concentration of metabolites should occur in the network vicinity of metabolic enzymes with activity that was affected by altered phosphorylation as a result of deletion of the encoded kinase or phosphatase.

To test this hypothesis, we overlaid the quantified metabolites on a stoichiometric model of yeast metabolism for each yeast deletion strain (*14*). The stoichiometric model was used to calculate a pairwise distance matrix between enzymes and metabolites by means of the minimum number of connecting enzymatic reactions. Hence, we assessed the probability that a significant change in the phosphorylation state of the metabolic enzyme was associated with changes in the concentrations of the substrates or products of the reactions it catalyzes (relative to that of more distant metabolites). For each metabolic enzyme (*7*), we considered the total change in phosphorylation state as the sum of all increases or decreases in the abundance of phosphopeptides representing changes in phosphorylation at different sites on that enzyme. Only phosphorylation events above an arbitrary fold change cutoff were selected, yielding a binary association matrix between kinase or phosphatase deletion strains and phosphorylated metabolic enzymes. We estimated the probability that the largest changes in the concentrations of metabolites occurred at different distances (from one to seven enzymatic reactions) from the phosphorylated enzyme by determining the area under the curve (AUC) of the corresponding receiver operating characteristic (ROC) curve as an estimate of the trade-off between sensitivity and false discovery. A large AUC indicated that the magnitude of the change in concentration of metabolites in a yeast deletion strain was larger for substrates or products of reactions catalyzed by a differentially phosphorylated enzyme in the same yeast strain. A small AUC indicated that metabolic changes were randomly distributed among metabolites more distal to differentially phosphorylated enzymes in a given yeast strain. We found a higher probability (larger AUC) for changes in metabolite concentrations with one degree of separation from differentially phosphorylated enzymes (Fig. 5). To evaluate the statistical robustness of this observation, we selected a range of different fold change cutoffs (from 95 to 99.9%) representing metabolic enzymes with the largest changes in phosphorylation. At any cutoff, the AUC was progressively lower with increased distance from differentially phosphorylated enzymes (Fig. 5). This observation of proximal metabolic changes propagating from a differentially phosphorylated enzyme is consistent with the proximity of steady-state metabolite responses previously described for overexpression of individual enzymes in yeast (*37*).

## Identification of functional phosphorylated sites using locality scoring

We developed a "locality" scoring procedure to obtain insight about the functional roles of individual phosphorylated sites in metabolic enzymes. The computation of the locality score uses the network distance between the phosphorylated enzymes and metabolites to weigh the strength of the correlations between changes in phosphorylation of specific sites and changes in the concentration of metabolites across all the yeast deletion strains where phosphorylation of that site was detected. We used a permutation test to evaluate the statistical significance of the locality scores. In addition, because the activity of an enzyme can be determined by phosphorylation at multiple sites, we also computed locality scores for changes in the abundance of up to three phosphorylated peptides from the same enzyme. For 47 enzymes, we found significant locality scores, indicating that the change in phosphorylation of at least one site was accompanied by coherent metabolic changes in the network vicinity of the phosphorylated enzyme (Table 1).

Of the 24 metabolic enzymes reported in the literature to have phosphorylation-dependent functions (table S1), 16 showed detectable changes in phosphorylation in the phosphoproteomic analysis of kinase and phosphatase deletion strains (*7*), and thus could be tested by the locality

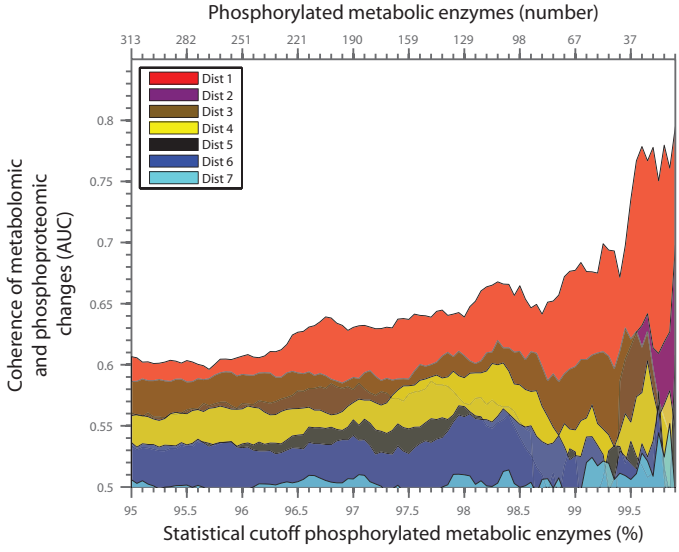


Fig. 5. Analysis of the network proximity of phosphoproteomic and metabolic changes. Values on the *x* axis are the percentage of metabolic enzymes with alterations in phosphorylation changes in each kinase or phosphatase deletion strain for a given fold change threshold calculated from the data in (*7*). For each threshold, a binary matrix of phosphorylated enzymes was compared to the metabolomics data for each strain by ROC analysis. Values on the *y* axis indicate the AUC index calculated for metabolites that are substrates or products of reactions at network distance between one and seven reactions. The larger the AUC, the stronger the association between phosphorylation and metabolic changes. An AUC of 0.5 corresponds to random associations.

scoring procedure. Of these, phosphorylation changes in nine metabolic enzymes—Acc1, Cki1, Gpd1, Gpd2, Gys2, Nha1, Pda1, Pfk2, and Tgl4 (*10*, *20*, *38*–*44*)—correlated with local metabolic changes (Table 1). Analysis of individual sites in three of these enzymes—Pda1, Gpd1, and Gpd2—correctly identified that phosphorylation of specific residues (and whether phosphorylation of one residue or several residues in combination) correlated with metabolic changes consistent with the annotated functions of these enzymes (table S10). For example, the locality score of $Ser^{313}$, but not $Tyr^{309}$, of Pda1 indicated that phosphorylation of this site was relevant to changes in the metabolic profiles across deletion strains (table S10), consistent with published data (*20*). Similarly, for Gpd1, combinations of phosphorylation of $Ser^{23}$, $Ser^{24}$, $Ser^{25}$, and $Ser^{27}$, but not phosphorylation at any one site, correlated with the expected changes in metabolite concentrations (table S10), consistent with published data (*10*). In the Gpd1 paralog

**Table 1. Results obtained from the locality scoring procedure.** Each row shows a phosphorylated metabolic enzyme in association with the minimum number of significant phosphosites predicted to affect its activity and the corresponding *P* value. Full details of the prediction including the amino acid sequence of the phosphorylated peptides are in table S10. The most probable direct regulators of these phosphorylated sites are shown in the last four columns according to (*7*). Fold change ($log_2$) indicates the phosphorylation changes relative to the corresponding reference wild-type strain. SGD, Saccharomyces Genome Database.

| Locus ID | SGD | Minimum number of phosphopeptides combinations | Most significant *P* value | Phosphatase | Phosphosite fold change ($log_2$) | Kinase | Phosphosite fold change ($log_2$) |
|---|---|---|---|---|---|---|---|
| yar042w | SWH1 | 1 | 0.001 | PPS1 | 1.931 | VPS15 | –1.857 |
| ybr023c | CHS3 | 1 | 0.001 | PPT1 | 0.882 | TPK2 | –0.882 |
| ydl019c | OSH2 | 1 | 0.001 | YVH1 | 1.064 | VPS34 | –1.409 |
| ydl131w | LYS21 | 1 | 0.001 | SIW14 | 1.567 | CMK1 | –1.824 |
| ydl182w | LYS20 | 1 | 0.001 | YVH1 | 2.081 | PHO85 | –4.152 |
| yel063c | CAN1 | 1 | 0.001 | PTC4 | 0.496 | YPK1 | –1.18 |
| ygl009c | LEU1 | 1 | 0.001 | SIW14 | 2.004 | TOS3 | –1.985 |
| yhr005c | GPA1 | 1 | 0.001 | PTC1 | 0.05 | PKH3 | –2.209 |
| yhr073w | OSH3 | 1 | 0.001 | PTC3 | 0.658 | KIN82 | –0.804 |
| Yil074c | SER33 | 1 | 0.001 | CNA1 | 0.096 | ELM1 | –0.863 |
| Yil105c | SLM1 | 1 | 0.001 | YCR079W | 1.162 | PKH3 | –5.342 |
| ykr067w | GPT2 | 1 | 0.001 | SIW14 | 0.196 | SNF1 | –2.966 |
| Ylr134w | PDC5 | 1 | 0.001 | PTC4 | 3.809 | KNS1 | –1.88 |
| Ylr138w | NHA1 | 1 | 0.001 | CMP2 | 1.131 | BUD32 | –2.46 |
| yml100w | TSL1 | 1 | 0.001 | YCR079W | 1.937 | MCK1 | –9.811 |
| ynl267w | PIK1 | 1 | 0.001 | YVH1 | 0.805 | RCK2 | –1.16 |
| ynl323w | LEM3 | 1 | 0.001 | PPS1 | 0.632 | RCK2 | –1.229 |
| ykl104c | GFA1 | 2 | 0.001 | YGR203W | 2.397 | HSL1 | –1.025 |
| Ylr142w | PUT1 | 1 | 0.001 | YGR203W | 0.896 | BUB1 | –1.319 |
| ydl022w | GPD1 | 3 | 0.002 | PTP1 | 2.336 | CTK1 | –4.141 |
| ygr240c | PFK1 | 1 | 0.002 | PPS1 | 2.363 | RCK2 | –2.358 |
| yor109w | INP53 | 1 | 0.002 | SIW14 | 0.592 | HRR25 | –0.534 |
| yer052c | HOM3 | 1 | 0.003 | SIT4 | 1.411 | YKL171W | –3.395 |
| ydr508c | GNP1 | 1 | 0.006 | PTC1 | 1.289 | PTK1 | –7.352 |
| ymr105c | PGM2 | 1 | 0.007 | PPQ1 | 1.12 | PKP1 | –4.517 |
| ypr159w | KRE6 | 2 | 0.007 | SIW14 | 0.635 | BUD32 | –1.639 |
| ybr069c | TAT1 | 1 | 0.008 | PSR1 | 2.562 | YPK2 | –2.819 |
| ynr016c | ACC1 | 1 | 0.008 | PTC7 | 0.992 | SPS1 | –1.761 |
| ygr267c | FOL2 | 1 | 0.009 | SIW14 | 0.959 | YKL161C | –0.64 |
| ymr011w | HXT2 | 1 | 0.013 | SIW14 | 0.65 | YPK2 | –2.059 |
| yal012w | CYS3 | 1 | 0.015 | PTP2 | 0.173 | PRK1 | –1.239 |
| ybl064c | PRX1 | 1 | 0.016 | YGR203W | 2.119 | SWE1 | –1.211 |
| ydl055c | PSA1 | 1 | 0.019 | PTC1 | 0.434 | HSL1 | –1.214 |
| ymr261c | TPS3 | 1 | 0.021 | PTC5 | 0.959 | CTK1 | –2.696 |
| yhr094c | HXT1 | 1 | 0.022 | CNA1 | 3.438 | HOG1 | –6.643 |
| ydr017c | KCS1 | 1 | 0.025 | PTC7 | 0.454 | PTK1 | –1.85 |
| Ylr133w | CKI1 | 1 | 0.027 | PPH21 | 2.409 | YPK1 | –2.019 |
| Ylr258w | GSY2 | 1 | 0.029 | PPH21 | 2.711 | MCK1 | –8.968 |
| ymr205c | PFK2 | 1 | 0.029 | PPH3 | 1.109 | SNF1 | –2.31 |
| ydr127w | ARO1 | 1 | 0.03 | PPQ1 | –0.509 | TPK1 | –1.109 |
| yol061w | PRS5 | 1 | 0.03 | SIT4 | 0.878 | PSK1 | –2.504 |
| Yll048c | YBT1 | 2 | 0.035 | OCA1 | 0.116 | SPS1 | –1.772 |
| ykl188c | PXA2 | 1 | 0.038 | CNA1 | 0.908 | PKP1 | –1.141 |
| ykr089c | TGL4 | 1 | 0.039 | PSR1 | 1.654 | ELM1 | –1.392 |
| yol059w | GPD2 | 1 | 0.04 | YVH1 | 1.474 | AKL1 | –3.216 |
| yer178w | PDA1 | 1 | 0.048 | PTC7 | 0.732 | PKP1 | –10.47 |
| ycr034w | FEN1 | 1 | 0.05 | PPH3 | 1.912 | MCK1 | –4.357 |

Gpd2, a change in the phosphorylation of one site was sufficient to yield local metabolic changes; however, the locality score of metabolic changes had a smaller *P* value when multiple sites on Gpd2 were phosphorylated (table S10), suggesting that multiple phosphorylation events are important for the activity of Gpd2, consistent with published results (*39*).

For the other metabolic enzymes with reported phosphorylation-dependent function, we observed different relationships between the phosphoproteomic and metabolomic changes. For example, in Nha1 or Pfk2, phosphorylation of the known site was predictive of metabolic changes only when in combination with phosphorylation of at least one additional site. Phosphorylation of $Thr^{765}$ and $Thr^{876}$ promotes the activity of Nha1 (*40*), and these sites were only detected in doubly phosphorylated peptides ($Thr^{765}$ and $Ser^{768}$ or $Thr^{874}$ and $Thr^{876}$), and phosphorylation of these sites in combination with phosphorylation of $Ser^{478}$ or $Ser^{479}$ correlated with metabolic changes (table S10). Mutation of $Ser^{163}$ inhibits the activity of Pfk2 (*10*), but none of the detected singly phosphorylated peptides ($Ser^{163}$, $Ser^{167}$, $Ser^{171}$, or $Tyr^{172}$) had a significant locality score. However, combinations of two or more phosphorylated sites that included $Ser^{167}$ correlated with metabolic changes across yeast deletion strains (table S10). The predictive value of phosphorylation of individual sites in Cki1, Gys2, and Tgl4 that are phosphorylated could not be tested because of lack of data from the phosphoproteomics analysis.

Thus, the agreement of the locality score–based predictions with published data supported the ability of this computational approach to predict previously uncharacterized phosphorylation-dependent regulation of metabolic enzyme activity and suggested that the other 38 enzymes with significant locality scores (Table 1) are candidates in which phosphorylation is likely to play a role in modulating their metabolic activity. For example, although phosphorylation of Acc1 is known to regulate its function (*38*, *45*), the specific site has not been reported, and the locality score analysis predicted that either $Ser^{1157}$ or $Ser^{1159}$ was likely to be the functionally relevant residue. In addition, 28 of these 38 enzymes undergo changes in phosphorylation in response to changes in the environmental conditions of yeast (*10*), suggesting that these enzymes may modulate metabolic responses to external stimuli.

## Phosphorylation of enzymes involved in lysine metabolism

We found that lysine biosynthesis was one of the most frequently affected pathways in yeast deletion strains in our metabolomics screen (Fig. 1B). In yeast, lysine biosynthesis is enhanced by the DNA binding transcriptional factor $Lys^{14}$ and modulated by allosteric feedback control from multiple pathway intermediates (*46*–*49*). The homocitrate synthase isoenzymes $Lys^{20}$ and $Lys^{21}$ catalyze the first step in lysine biosynthesis, converting oxoglutarate in homocitrate. The locality score analysis predicted that phosphorylation of $Ser^{409}$ on $Lys^{21}$ or phosphorylation of $Thr^{396}$, $Ser^{410}$, or both $Thr^{396}$ and $Ser^{410}$ on $Lys^{20}$ may affect the activity of these enzymes (table S10). To experimentally test these predictions, we replaced these residues with alanine to prevent phosphorylation or with glutamate to mimic constitutive phosphorylation. Plasmids encoding either the wild-type or the mutant $Lys^{20}$ or $Lys^{21}$ were transformed into yeast with knockout of both *LYS20* and *LYS21* (*lys20*Δ-*lys21*Δ), which do not grow without supplemental lysine in the medium (table S3). Nevertheless, even in the presence of supplemental lysine in the medium, the growth of *lys20*Δ-*lys21*Δ yeast was inhibited compared to wild-type yeast (fig. S4A), indicating that the amount of lysine supplemented in the medium is limiting. In contrast, *lys20*Δ-*lys21*Δ yeast complemented with wild-type $Lys^{20}$ or $Lys^{21}$ had growth rates similar to wild-type yeast in the absence of supplemental lysine (fig. S4A). Moreover, *lys20*Δ-*lys21*Δ yeast complemented with mutant $Lys^{20}$ (fig. S4B) or mutant $Lys^{21}$ (fig. S4C) showed growth rates similar to that of *lys20*Δ-*lys21*Δ yeast complemented with wild-type $Lys^{20}$ or $Lys^{21}$ in the absence of supplemental lysine, suggesting that changes in the phosphorylation state of homocitrate synthases may not affect lysine biosynthesis or that compensatory mechanisms may account for disruption of the phosphorylation-dependent regulation of these enzymes.

Thus, we monitored metabolite concentrations in *lys20*Δ-*lys21*Δ yeast complemented with wild-type or mutant $Lys^{20}$ or $Lys^{21}$ in the absence of supplemental lysine. Compared to *lys20*Δ-*lys21*Δ yeast transformed with wild-type $Lys^{20}$, those transformed with $Lys^{20}$-T396A, but not $Lys^{20}$-S395A, had increased concentration of lysine and homocitrate (Fig. 6, A and B). In contrast, *lys20*Δ-*lys21*Δ yeast transformed with $Lys^{20}$ [S395E-T396E-S410E] had a slight, but statistically significant, decrease in the concentration of lysine (Fig. 6A). Expression of mutant $Lys^{21}$ in *lys20*Δ-*lys21*Δ yeast did not affect the concentration of homocitrate, whereas expression of either $Lys^{21}$-S409A or $Lys^{21}$[S409E-T410E] in these yeast reduced the concentration of lysine, relative to expression of wild-type $Lys^{21}$ in these yeast (Fig. 6A). Thus, both $Lys^{20}$ and $Lys^{21}$ contribute to lysine biosynthesis, and phosphorylation may inhibit $Lys^{20}$ activity. Among the kinase and phosphatase yeast deletion strains, in *pho85*Δ yeast, we found a fourfold increase in the concentration of lysine (Table 1) and a fourfold reduction of phosphorylation of $Lys^{20}$ (Table 1), suggesting that Pho85 may inhibit lysine production through phosphorylation of $Lys^{20}$.

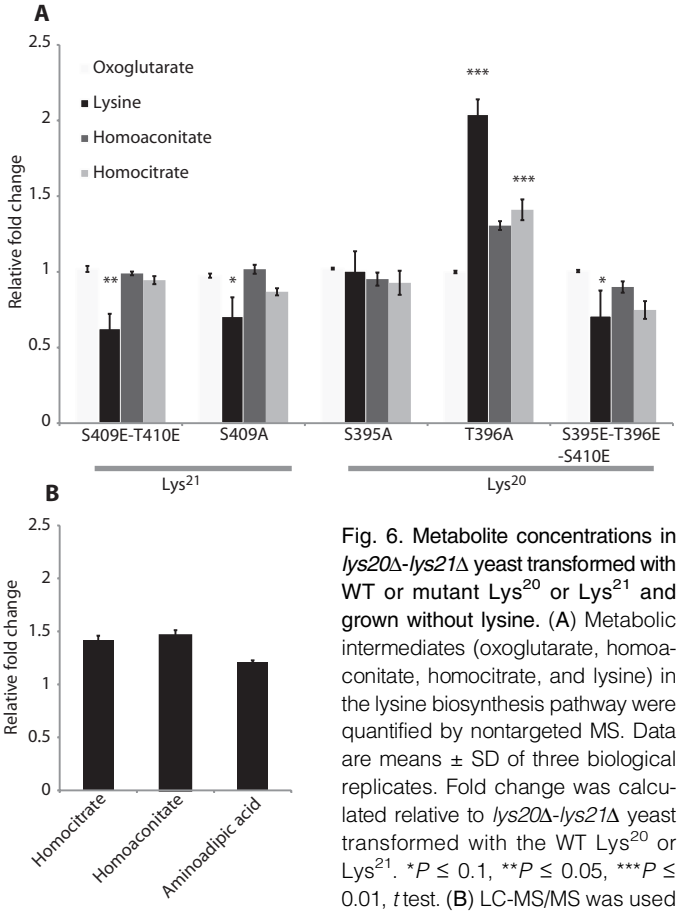


Fig. 6. Metabolite concentrations in *lys20*Δ-*lys21*Δ yeast transformed with WT or mutant $Lys^{20}$ or $Lys^{21}$ and grown without lysine. (A) Metabolic intermediates (oxoglutarate, homoaconitate, homocitrate, and lysine) in the lysine biosynthesis pathway were quantified by nontargeted MS. Data are means ± SD of three biological replicates. Fold change was calculated relative to *lys20*Δ-*lys21*Δ yeast transformed with the WT $Lys^{20}$ or $Lys^{21}$. $^{*}P \leq 0.1$, $^{**}P \leq 0.05$, $^{***}P \leq 0.01$, *t* test. (B) LC-MS/MS was used to confirm the accumulation of lysine synthesis intermediates in the *lys20*Δ-*lys21*Δ expressing $Lys^{20}$-T309A compared to those expressing WT $Lys^{20}$. Data are means ± SD of three biological replicates.

## DISCUSSION

By monitoring the changes in concentrations of hundreds of intracellular metabolites in response to genetic perturbations of the yeast kinome, we probed functionality of kinases and phosphates in modulating metabolic processes. Whereas single kinase or phosphatase deletions often had no growth phenotypes, we found that metabolite concentrations were sensitive and informative phenotypic readouts. Nevertheless, even for the single, tested steady-state condition, about two-thirds of the kinase and phosphate deletion strains exhibited altered metabolic profiles. Evaluation of data by van Wageningen *et al*. (*9*), using statistical criteria similar to those applied in the current study, revealed that only 26% of kinase or phosphatase deletion strains showed significant transcriptional changes, suggesting that the metabolic changes we observed in these yeast deletion strains may primarily reflect the role of phosphorylation in modulating enzyme activity, rather than the indirect consequence of changes in transcription.

By defining the metabolomic profiles of kinase and phosphatase deletion strains in yeast and mapping the changes to metabolic pathways, we investigated the role of phosphorylation in metabolic regulation. We predicted specific regulatory roles for six kinases and phosphatases. Two deletions—*rim11*Δ and *smk1*Δ—selectively affected tryptophan metabolism indicated by reduced amounts of kynurenic acid. The metabolism of kynurenic acid plays an important role in various pathologies of the central nervous system (*50*, *51*). Yeast SMK1 has sequence homology to human ERK5 (extracellular signal–regulated kinase 5), a member of the MAP kinase family involved in a variety of biological processes, including brain development (*52*, *53*), suggesting that the relationship between homologs of SMK1 and kynurenic acid may be relevant in vertebrates.

Overall, we found that only a few deletion strains had alterations in metabolites involved in central metabolism. This result was unexpected given that mutation of individual phosphorylated sites in multiple central metabolic enzymes affects metabolite concentrations (*10*). Moreover, post-transcriptional regulation is key in modulating glycolytic flux in yeast (*54*). A possible explanation for this discrepancy is the existence of redundant kinases with the same or similar targets that could compensate for deletion of individual kinases (*7*, *9*). Furthermore, we used a nutritionally complex medium that favors glycolytic metabolism and exponential growth, which may not be representative of natural environments where more kinases and phosphatases may be essential (*55*). Moreover, phosphorylation of metabolic enzymes may be more crucial in mediating dynamic transitions between two steady states, but less important for maintaining steady-state metabolism (*56*, *57*).

An example of the importance of kinases and phosphatases in mediating the transition from one metabolic state to another was found in *ppq1*Δ yeast. Deletion of the gene encoding Ppq1 was the only low-impact deletion that caused alterations in the concentrations of metabolites within the TCA cycle, including citrate. Whereas the growth of *ppq1*Δ yeast was indistinguishable from wild-type yeast in most steady-state conditions, with a minor growth defect on ethanol, we unraveled the intrinsic importance of Ppq1 in transiently rewiring cellular networks during the diauxic shift from glucose to ethanol, which involves extensive changes in the activity of multiple enzymes involved in the TCA cycle (*58*). Ppq1 was required for Mn homeostasis, which may have indirect effects on the TCA cycle through the effect of Mn on the activities of enzymes governing citrate metabolism (*32*, *59*–*61*), including Aco1 (*62*, *63*). Reduced dephosphorylation of Aco1 in *ppq1*Δ yeast could inhibit the conversion of citrate to isocitrate, leading to the accumulation of citrate (*64*). Citrate can chelate divalent metal ions (*65*) and, thus, may also play a direct role in metal homeostasis, protecting cells from excess Mn, similar to the role of citrate in tolerance to excess aluminum (*66*).

The developed experimental-computational approach enabled us to assess the role of phosphorylation in regulating metabolic functions on a proteome-wide scale. Identifying roles of kinases and phosphatases in metabolism and the relevant phosphorylated sites in metabolic enzymes has high value in expanding our current knowledge on the mechanisms by which phosphorylation regulates diverse cellular functions.

## MATERIALS AND METHODS

### Strains and cultivation

*S. cerevisiae* strains corresponding to individual deletions of 91 kinases and 27 phosphatases were obtained from (*7*). We removed one strain (*ssn3*Δ) because of extremely slow growth. Cultures were grown in a synthetic defined medium prepared as in (*7*), containing 1.7 g of yeast nitrogen base without amino acids and ammonium sulfate (Chemie Brunschwig), 5 g of ammonium sulfate, 20 g of glucose, 0.03 g of isoleucine, 0.15 g of valine, 0.04 g of adenine, 0.02 g of arginine, 0.02 g of histidine, 0.1 g of leucine, 0.03 g of lysine, 0.02 g of methionine, 0.05 g of phenylalanine, 0.2 g of threonine, 0.04 g of tryptophan, 0.03 g of tyrosine, 0.02 g of uracil, 0.1 g of glutamic acid, and 0.1 g of aspartic acid per liter. Medium prepared with yeast nitrogen base contained $MnSO_4$ (400 μg/liter). For growth without lysine, the same medium was prepared without lysine. The prototrophic *ppq1*Δ and respective wild-type reference JHY222 strains were provided by A. Chu and J. Horecka (Stanford University) and cultivated in Verduyn minimal medium (*67*) with either glucose (20 g/liter), galactose (20 g/liter), or ethanol (15.4 g/liter) as the sole carbon source. Verduyn medium contains $MnCl_2$ $4H_2O$ (1 mg/liter). In the diauxic shift experiment, wild-type and *ppq1*Δ yeast strains were grown in Verduyn minimal medium with glucose as carbon source.

To generate the *LYS20* and *LYS21* double deletion strain, we first replaced the kanamycin resistance cassette (KanMX) in *lys20*Δ yeast with the nourseothricin resistance cassette (NatMX) by transformation and homologous recombination. We used DNA from the resulting *lys20*Δ (NatMX) strain as a template for the polymerase chain reaction (PCR)–based amplification of the NatMX cassette including at least 200 base pairs of the flanking region of the *LYS20* gene. The resulting DNA amplicon was transformed into *lys21*Δ (KanMX) to obtain *lys20*Δ (NatMX)–*lys21*Δ (KanMX). Transformants were selected on yeast peptone dextrose (YPD) plates containing nourseothricin (100 mg/liter) and geneticin (200 mg/liter) (G418). Plasmids carrying mutations of *LYS20* or *LYS21* were generated by first cloning the wild-type sequence (*68*), including the native promoter region, into the vector pRS416 that contains the *ura3* selection marker. Single-site mutated variants were generated by whole-plasmid PCR with the QuikChange Site-Directed Mutagenesis Kit (Roche), and all constructs were verified by sequencing. The triple phosphosite mutation $Lys^{20}$[S395E-T396E-S410E] and the double phosphosite mutation $Lys^{21}$[S409E-T410E] were purchased from GenScript. Plasmids were transformed into the *lys20*Δ-*lys21*Δ strain, and positive transformants were selected on –ura plates [containing glutamate (1 g/liter) as nitrogen source] containing nourseothricin (100 mg/liter) and geneticin (200 mg/liter) (G418).

### Nontargeted metabolomic profiling by TOF MS

Deep 96-well cultures of 1.2 ml were inoculated independently for each deletion strain to an initial density precalculated to achieve an $OD_{595}$ (optical density at 595 nm) of 1 after strains had grown for a period of time

corresponding to at least two wild-type doubling times. Six replicates of each deletion strain and 12 replicates of the appropriate wild-type reference were grown on the same plate. When the wells reached an $OD_{595}$ of 1 ± 0.4, the plates were centrifuged for 1 min at 0°C, the supernatant medium was discarded, and 150 µl of 80°C extraction solution [75% (v/v) ethanol, 10 mM ammonium acetate at pH 7.5] was added to each well. Metabolites were extracted by incubation at 80°C in a water bath for 5 min. Metabolites were analyzed by direct flow injection on a platform consisting of an Agilent Series 1100 LC pump coupled to a GERSTEL MPS2 autosampler and an Agilent 6520 series quadrupole TOF MS scanning a mass/charge ratio (*m/z*) range of 50 to 1000 as described (*13*). Ions were annotated by searching possible matching metabolites in the KEGG database (http://www.genome.jp/kegg/) or in the genome-wide reconstruction of yeast metabolism by (*14*). Neutrally charged metabolites were annotated as described in (*13*). Full details of the annotation are provided in table S2.

## Targeted metabolomic profiling by LC-MS/MS

Targeted quantification of citrate, aconitate, homocitrate, homoaconitate, and aminoadipate was performed by ion pairing reverse-phase chromatography separation and LC-MS/MS detection (*69*). Chromatography was performed on a Waters ACQUITY UPLC using an end-capped reverse phase coupled to a TSQ Quantum Ultra Triple Quadrupole MS (Thermo Fisher Scientific). The homocitrate assay is specific for the isomer homocitrate and excludes the isomer methylcitrate. The homoaconitate assay also measures the isomer methylaconitate. For the aminoadipate assay, no isomers have been evaluated. Peak areas were integrated as described (*13*) and normalized to levels of fully $^{13}$C-labeled citrate from the internal standard.

## Comparative differential analysis

Permutation analysis was used to assess significance of the differential abundance of ions between deletion and the appropriate control strains (table S3). For each ion (*i*), we calculated the difference between the mean intensity within the pool of replicates for each deletion strain ($X_{ij}$) and the pool of biological replicates of the respective reference wild type ($X_{ir}$) grown in the same 96-well plate. The assigned *P* value ($Pval_{ij}$) was based on 10,000 permutations where the deletion strain and wild-type replicates were randomly shuffled between the two groups ($X^k_{ij}$ and $X^k_{ir}$):

$$P_{val^x_{ij}} = \frac{\sum_{k=1}^{K} I\{|\tilde{X}^k_{ij} - \tilde{X}^k_{ir}| \geq |X_{ij} - X_{ir}|\}}{K}$$

$$fc_{ij} = \log_2 \frac{X_{ij}}{X_{ir}}$$

where $fc_{ij}$ represented $\log_2$ fold change in intensity of ion *i* between deletion *j* and reference *r*, and *K* was the number of permutations performed. *P* values were corrected for multiple tests using a false discovery rate approximation using the MATLAB MaDfr function as described (*70*). To determine an appropriate fold change cutoff accounting for the intrinsic noise in the experimental and measurement protocols, we generated a background distribution of fold changes across plates by randomly selecting six wild-type replicates and comparing the mean ion intensity to that of the other six wild-type replicates on each 96-well plate (fig. S5). A $\log_2$ fold change cutoff greater than or equal to 0.8 produced a false discovery rate less than 1%. In addition, combining the 0.8 fold change cutoff with a corrected *P* value cutoff of less than or equal to 0.001 resulted in a false discovery rate of 0.00044%.

## Clustering and pathway enrichment

The number of ions with significant (fold change ≥0.8 and $P \leq 0.001$) changes in intensity in a yeast deletion strain was used to determine the metabolic impact (table S4). The four different impact groups (silent, low, average, and high) were classified using a hypergeometric probability density function (fig. S1B). We considered deletion strains with 24 to 48 affected metabolites as average impact (deletion strains that showed the expected number of hits), those with fewer than 24 affected metabolites as low impact, and those with 48 or more affected metabolites as high impact.

Clustering of metabolomic profiles (table S4) was performed by an affinity propagation algorithm (*16*). We used the fold change matrix for all ions as input and Euclidian distance to evaluate similarity between deletion strains. The damping factor was set to 0.5. We performed an analysis to determine whether the kinases and phosphatases corresponding to the deletion strains in each cluster were enriched for interactions (considering all possible types of interactions) annotated in the STRING database (http://string-db.org/). We used a hypergeometric test to calculate the *P* value.

Enrichment or depletion of GO terms within genes from a cluster was evaluated using the tool GOstats 2.26 within R 3.01[45]. *P* values for all conditional terms were calculated with a Fisher's exact test, including corrections for multiple testing (Benjamini-Hochberg). Terms inferred from electronic annotation (IEA) were included into the analysis. Mapping to GO slim terms was performed unconditionally with the map2slim package. We used all genes from all clusters as a background.

To determine whether differentially regulated metabolites in a given deletion strain were enriched in a metabolic pathway using KEGG pathway annotations (table S7), we calculated the *P* value using a permutation analysis. We repetitively (1000 times) randomly shuffled the associations between detected ions and corresponding annotated metabolites. For each random permutation, we estimated the overrepresentation of metabolites in each KEGG pathway. Pathway enrichments for the experimental metabolite annotations (table S2) were compared to those for the randomly generated annotations, and pathways with $P < 0.05$ were considered enriched.

## Locality scoring procedure

A genome-scale network model of yeast metabolism (*14*) was used to determine the distance between each enzyme-metabolite pair. The resulting pairwise distance matrix between metabolic enzymes and metabolites was estimated by means of the minimum number of reactions separating the two in a nondirectional network. We derived the distance matrix between metabolites by multiplying the stoichiometric matrix (*V*) by its transpose, and then subsequently applying a standard implementation of the Dijkstra algorithm. All highly connected metabolites were removed before calculation (table S2). For each enzyme with a change in the abundance of a phosphopeptide in at least five different kinase or phosphatase deletion strains according to (*7*), we calculated the correlations between the fold change of abundance of the phosphopeptide and the fold change of the concentrations of each metabolite ($\log_2$ fold change ion intensity). This computation results in a matrix *C* of correlations between metabolic enzyme phosphorylation changes (rows) and metabolite changes (columns) across all deletion strains. To achieve high coverage of the metabolic network, we used all ions annotated as neutral losses (table S2). To test the possibility that changes in the phosphorylation of metabolic enzymes at individual sites were not sufficient to alter its activity, we used a linear multiple regression scheme where all possible combinations of up to a maximum of three phosphopeptides located in the same protein were tested against all annotated metabolite profiles. In these cases, correlation with the best linear fit was used. Finally, we calculated the locality score (table S10) to assess the

proximity of coherent phosphorylation and metabolic changes for each metabolic enzyme using the following weighted scoring function:

$$S(P_i) = \frac{\sum_{m=1}^{M} D_{i,m}^{-2} \cdot (1 - \mathrm{Pval}_{C_{i,m}}) \cdot |C_{i,m}|}{\sum_{m=1}^{M} D_{i,m}^{-2} \cdot (1 - \mathrm{Pval}_{C_{i,m}})}$$

$i$ = index phosphopeptide combination
$m$ = index metabolite
$p$ = phosphopeptide
$S(p_i)$ = locality score for $p_i$
$C_{i,m}$ = Spearman correlation coefficient between $p_i$ and $m$
$D_{i,m}$ = network distance between the $i$ and $m$
$\mathrm{Pval}_{C_{i,m}}$ = $P$ value of $C_{i,m}$.

For each combination of phosphopeptides $p_i$, a weighted mean over corresponding $C_{i,m}$ is computed. Weights are a function of the inverse of the distance between the enzyme, where the phosphopeptide $i$ was detected and the metabolite ($m$) to the power two ($D_{i,m}$) and the resulting $P$ value of the estimated correlation $\mathrm{Pval}_{C_{i,m}}$. Significance of the final score was assessed by random permutation of the distance matrix $D$ ($D_{\mathrm{rand}}$) 1000 times as follows:

$$S^k_{\mathrm{rand}}(p_i) = \frac{\sum_{m=1}^{M} (D^k_{\mathrm{rand}_{i,m}})^{-2} \cdot (1 - C.\mathrm{Pval}_{i,m}) \cdot |C_{i,m}|}{\sum_{m=1}^{M} (D^k_{\mathrm{rand}_{i,m}})^{-2} \cdot (1 - C.\mathrm{Pval}_{i,m})}$$

$$\mathrm{p.value}(p_i) = \frac{\sum_k (S^k_{\mathrm{rand}} \geq S)}{K}$$

$k$ = index permutation
$K$ = number of permutations (1000 permutations used in this study)
$S^k_{\mathrm{rand}}(p_i)$ = locality score for phosphopeptide combination $p_i$ based on a randomized distance matrix
$D_{\mathrm{rand}}$ = randomly shuffled the distance matrix $D$.

## SUPPLEMENTARY MATERIALS

www.sciencesignaling.org/cgi/content/full/7/353/rs6/DC1
Fig. S1. Impact of kinase and phosphatase deletions on the metabolome.
Fig. S2. Number of enriched metabolic pathways per deletion strain.
Fig. S3. Growth profiles of yeast expressing mutant $Lys^{20}$ or $Lys^{21}$.
Fig. S4. Calculation of statistical threshold for metabolomic profiles.
Fig. S5. Schematic representation of the experimental setup and analysis workflow.
Table S1. Enzymes regulated by phosphorylation.
Table S2. Details of MS ion annotation.
Table S3. Fold change matrix of metabolite ion intensities.
Table S4. Growth rate, metabolic impact, and metabolic similarity of kinase and phosphatase deletion strains.
Table S5. GO enrichments for impact groups.
Table S6. GO enrichments and STRING interactions for clusters.
Table S7. KEGG pathway enrichment analysis of altered metabolites in kinase and phosphatase deletion strains.
Table S8. Growth rates of *ppq1*Δ yeast grown on different carbon sources.
Table S9. Phosphoproteomic changes in *ppq1*Δ yeast.
Table S10. Predictions from locality scoring procedure.

## REFERENCES AND NOTES


1. A. Breitkreutz, H. Choi, J. R. Sharom, L. Boucher, V. Neduva, B. Larsen, Z. Y. Lin, B. J. Breitkreutz, C. Stark, G. Liu, J. Ahn, D. Dewar-Darch, T. Reguly, X. Tang, R. Almeida, Z. S. Qin, T. Pawson, A. C. Gingras, A. I. Nesvizhskii, M. Tyers, A global protein kinase and phosphatase interaction network in yeast. *Science* **328**, 1043–1046 (2010).
2. N. E. Hynes, P. W. Ingham, W. A. Lim, C. J. Marshall, J. Massagué, T. Pawson, Signalling change: Signal transduction through the decades. *Nat. Rev. Mol. Cell Biol.* **14**, 393–398 (2013).
3. H. Zhu, J. F. Klemic, S. Chang, P. Bertone, A. Casamayor, K. G. Klemic, D. Smith, M. Gerstein, M. A. Reed, M. Snyder, Analysis of yeast protein kinases using protein chips. *Nat. Genet.* **26**, 283–289 (2000).
4. S. S. Taylor, M. M. Keshwani, J. M. Steichen, A. P. Kornev, Evolution of the eukaryotic protein kinases as dynamic molecular switches. *Philos. Trans. R. Soc. Lond. B Biol. Sci.* **367**, 2517–2528 (2012).
5. H. S. Meharena, P. Chang, M. M. Keshwani, K. Oruganty, A. K. Nene, N. Kannan, S. S. Taylor, A. P. Kornev, Deciphering the structural basis of eukaryotic protein kinase regulation. *PLOS Biol.* **11**, e1001680 (2013).
6. J. Mok, H. Im, M. Snyder, Global identification of protein kinase substrates by protein microarray analysis. *Nat. Protoc.* **4**, 1820–1827 (2009).
7. B. Bodenmiller, S. Wanka, C. Kraft, J. Urban, D. Campbell, P. G. Pedrioli, B. Gerrits, P. Picotti, H. Lam, O. Vitek, M. Y. Brusniak, B. Roschitzki, C. Zhang, K. M. Shokat, R. Schlapbach, A. Colman-Lerner, G. P. Nolan, A. I. Nesvizhskii, M. Peter, R. Loewith, C. von Mering, R. Aebersold, Phosphoproteomic analysis reveals interconnected system-wide responses to perturbations of kinases and phosphatases in yeast. *Sci. Signal.* **3**, rs4 (2010).
8. S. Sharifpoor, D. van Dyk, M. Costanzo, A. Baryshnikova, H. Friesen, A. C. Douglas, J. Y. Youn, B. VanderSluis, C. L. Myers, B. Papp, C. Boone, B. J. Andrews, Functional wiring of the yeast kinome revealed by global analysis of genetic network motifs. *Genome Res.* **22**, 791–801 (2012).
9. S. van Wageningen, P. Kemmeren, P. Lijnzaad, T. Margaritis, J. J. Benschop, I. J. de Castro, D. van Leenen, M. J. A. Groot Koerkamp, C. W. Ko, A. J. Miles, N. Brabers, M. O. Brok, T. L. Lenstra, D. Fiedler, L. Fokkens, R. Aldecoa, E. Apweiler, V. Taliadouros, K. Sameith, L. A. L. van de Pasch, S. R. van Hooff, L. V. Bakker, N. J. Krogan, B. Snel, F. C. P. Holstege, Functional overlap and regulatory links shape genetic interactions between signaling pathways. *Cell* **143**, 991–1004 (2010).
10. A. P. Oliveira, C. Ludwig, P. Picotti, M. Kogadeeva, R. Aebersold, U. Sauer, Regulation of yeast central metabolism by enzyme phosphorylation. *Mol. Syst. Biol.* **8**, 623 (2012).
11. H. Daub, J. V. Olsen, M. Bairlein, F. Gnad, F. S. Oppermann, R. Körner, Z. Greff, G. Kéri, O. Stemmann, M. Mann, Kinase-selective enrichment enables quantitative phosphoproteomics of the kinome across the cell cycle. *Mol. Cell* **31**, 438–448 (2008).
12. C. Stark, T. C. Su, A. Breitkreutz, P. Lourenco, M. Dahabieh, B. J. Breitkreutz, M. Tyers, I. Sadowski, PhosphoGRID: A database of experimentally verified in vivo protein phosphorylation sites from the budding yeast *Saccharomyces cerevisiae*. *Database J. Biol. Databases Curation* **2010**, bap026 (2010).
13. T. Fuhrer, D. Heer, B. Begemann, N. Zamboni, High-throughput, accurate mass metabolome profiling of cellular extracts by flow injection-time-of-flight mass spectrometry. *Anal. Chem.* **83**, 7074–7080 (2011).
14. P. D. Dobson, K. Smallbone, D. Jameson, E. Simeonidis, K. Lanthaler, P. Pir, C. Lu, N. Swainston, W. B. Dunn, P. Fisher, D. Hull, M. Brown, O. Oshota, N. J. Stanford, D. B. Kell, R. D. King, S. G. Oliver, R. D. Stevens, P. Mendes, Further developments towards a genome-scale metabolic model of yeast. *BMC Syst. Biol.* **4**, 145 (2010).
15. M. Kanehisa, S. Goto, KEGG: Kyoto Encyclopedia of Genes and Genomes. *Nucleic Acids Res.* **28**, 27–30 (2000).
16. B. J. Frey, D. Dueck, Clustering by passing messages between data points. *Science* **315**, 972–976 (2007).
17. D. Szklarczyk, A. Franceschini, M. Kuhn, M. Simonovic, A. Roth, P. Minguez, T. Doerks, M. Stark, J. Muller, P. Bork, L. J. Jensen, C. von Mering, The STRING database in 2011: Functional interaction networks of proteins, globally integrated and scored. *Nucleic Acids Res.* **39**, D561–D568 (2011).
18. A. A. Sneddon, P. T. Cohen, M. J. Stark, *Saccharomyces cerevisiae* protein phosphatase 2A performs an essential cellular function and is encoded by two genes. *EMBO J.* **9**, 4339–4346 (1990).
19. T. Toda, S. Cameron, P. Sass, M. Zoller, M. Wigler, Three different genes in S. cerevisiae encode the catalytic subunits of the cAMP-dependent protein kinase. *Cell* **50**, 277–287 (1987).
20. U. Gey, C. Czupalla, B. Hoflack, G. Rödel, U. Krause-Buchholz, Yeast pyruvate dehydrogenase complex is regulated by a concerted activity of two kinases and two phosphatases. *J. Biol. Chem.* **283**, 9759–9767 (2008).
21. T. J. Westmoreland, S. M. Wickramasekara, A. Y. Guo, A. L. Selim, T. S. Winsor, A. L. Greenleaf, K. L. Blackwell, J. A. Olson, J. R. Marks, C. B. Bennett, Comparative genome-wide screening identifies a conserved doxorubicin repair network that is diploid specific in *Saccharomyces cerevisiae*. *PLOS One* **4**, e5830 (2009).
22. L. C. Robinson, E. J. Hubbard, P. R. Graves, A. A. DePaoli-Roach, P. J. Roach, C. Kung, D. W. Haas, C. H. Hagedorn, M. Goebl, M. R. Culbertson, Yeast casein kinase I homologues: An essential gene pair. *Proc. Natl. Acad. Sci. U.S.A.* **89**, 28–32 (1992).
23. Y. Wang, H. G. Dohlman, Pheromone signaling mechanisms in yeast: A prototypical sex machine. *Science* **306**, 1508–1509 (2004).
24. P. M. B. Fernandes, A. D. Panek, Pheromone response in trehalose-6-phosphate synthase yeast mutants. *Microbiology* **143**, 689–690 (1997).
25. P. Chumnanpuen, J. Zhang, I. Nookaew, J. Nielsen, Integrated analysis of transcriptome and lipid profiling reveals the co-influences of inositol–choline and Snf1 in controlling lipid biosynthesis in yeast. *Mol. Genet. Genomics* **287**, 541–554 (2012).
26. S. Sharifpoor, A. N. Nguyen Ba, J. Y. Young, D. van Dyk, H. Friesen, A. C. Douglas, C. F. Kurat, Y. T. Chong, K. Founk, A. M. Moses, B. J. Andrews, A quantitative literature-curated gold standard for kinase-substrate pairs. *Genome Biol.* **12**, R39 (2011).

27. A. Vincent, G. Newnam, S. W. Liebman, The yeast translational allosuppressor, *SAL6*: A new member of the PP1-like phosphatase family with a long serine-rich N-terminal extension. *Genetics* **138**, 597–608 (1994).
28. N. Alic, V. J. Higgins, I. W. Dawes, Identification of a *Saccharomyces cerevisiae* gene that is required for G1 arrest in response to the lipid oxidation product linoleic acid hydroperoxide. *Mol. Biol. Cell* **12**, 1801–1810 (2001).
29. S. M. Fendt, A. P. Oliveira, S. Christen, P. Picotti, R. C. Dechant, U. Sauer, Unraveling condition-dependent networks of transcription factors that control metabolic pathway activity in yeast. *Mol. Syst. Biol.* **6**, 432 (2010).
30. J. S. Flick, J. Thorner, An essential function of a phosphoinositide-specific phospholipase C is relieved by inhibition of a cyclin-dependent protein kinase in the yeast *Saccharomyces cerevisiae*. *Genetics* **148**, 33–47 (1998).
31. L. T. Jensen, M. Ajua-Alemanji, V. C. Culotta, The *Saccharomyces cerevisiae* high affinity phosphate transporter encoded by *PHO84* also functions in manganese homeostasis. *J. Biol. Chem.* **278**, 42036–42040 (2003).
32. V. C. Culotta, M. J. Daly, Manganese complexes: Diverse metabolic routes to oxidative stress resistance in prokaryotes and yeast. *Antioxid. Redox Signal.* **19**, 933–944 (2013).
33. E. C. Chang, D. J. Kosman, Intracellular Mn (II)-associated superoxide scavenging activity protects Cu,Zn superoxide dismutase-deficient *Saccharomyces cerevisiae* against dioxygen stress. *J. Biol. Chem.* **264**, 12172–12178 (1989).
34. M. A. Farooq, T. M. Pracheil, Z. Dong, F. Xiao, Z. Liu, Mitochondrial DNA instability in cells lacking aconitase correlates with iron citrate toxicity. *Oxid. Med. Cell. Longev.* **2013**, 493536 (2013).
35. K. Murakami, M. Yoshino, Inactivation of aconitase in yeast exposed to oxidative stress. *Biochem. Mol. Biol. Int.* **41**, 481–486 (1997).
36. J. A. Baron, K. M. Laws, J. S. Chen, V. C. Culotta, Superoxide triggers an acid burst in *Saccharomyces cerevisiae* to condition the environment of glucose-starved cells. *J. Biol. Chem.* **288**, 4557–4566 (2013).
37. S. M. Fendt, J. M. Buescher, F. Rudroff, P. Picotti, N. Zamboni, U. Sauer, Tradeoff between enzyme and metabolite efficiency maintains metabolic homeostasis upon perturbations in enzyme capacity. *Mol. Syst. Biol.* **6**, 356 (2010).
38. A. Woods, M. R. Munday, J. Scott, X. Yang, M. Carlson, D. Carling, Yeast SNF1 is functionally related to mammalian AMP-activated protein kinase and regulates acetyl-CoA carboxylase in vivo. *J. Biol. Chem.* **269**, 19509–19515 (1994).
39. Y. J. Lee, G. R. Jeschke, F. M. Roelants, J. Thorner, B. E. Turk, Reciprocal phosphorylation of yeast glycerol-3-phosphate dehydrogenases in adaptation to distinct types of stress. *Mol. Cell. Biol.* **32**, 4705–4717 (2012).
40. M. Proft, K. Struhl, MAP kinase-mediated stress relief that precedes and regulates the timing of transcriptional induction. *Cell* **118**, 351–361 (2004).
41. M. G. Choi, V. Kurnov, M. C. Kersting, A. Sreenivas, G. M. Carman, Phosphorylation of the yeast choline kinase by protein kinase C. Identification of $Ser^{25}$ and $Ser^{30}$ as major sites of phosphorylation. *J. Biol. Chem.* **280**, 26105–26112 (2005).
42. Y. Yu, A. Sreenivas, D. B. Ostrander, G. M. Carman, Phosphorylation of *Saccharomyces cerevisiae* choline kinase on $Ser^{30}$ and $Ser^{85}$ by protein kinase A regulates phosphatidylcholine synthesis by the CDP-choline pathway. *J. Biol. Chem.* **277**, 34978–34986 (2002).
43. T. A. Hardy, P. J. Roach, Control of yeast glycogen synthase-2 by COOH-terminal phosphorylation. *J. Biol. Chem.* **268**, 23799–23805 (1993).
44. C. F. Kurat, H. Wolinski, J. Petschnigg, S. Kaluarachchi, B. Andrews, K. Natter, S. D. Kohlwein, Cdk1/Cdc28-dependent activation of the major triacylglycerol lipase Tgl4 in yeast links lipolysis to cell-cycle progression. *Mol. Cell* **33**, 53–63 (2009).
45. K. I. Mitchelhill, D. Stapleton, G. Gao, C. House, B. Michell, F. Katsis, L. A. Witters, B. E. Kemp, Mammalian AMP-activated protein kinase shares structural and functional homology with the catalytic domain of yeast Snf1 protein kinase. *J. Biol. Chem.* **269**, 2361–2364 (1994).
46. M. El Alami, A. Feller, A. Piérard, E. Dubois, The proper folding of a long C-terminal segment of the yeast Lys14p regulator is required for activation of *LYS* genes in response to the metabolic effector. *Mol. Microbiol.* **43**, 1629–1639 (2002).
47. A. Feller, E. Dubois, F. Ramos, A. Piérard, Repression of the genes for lysine biosynthesis in *Saccharomyces cerevisiae* is caused by limitation of Lys14-dependent transcriptional activation. *Mol. Cell. Biol.* **14**, 6411–6418 (1994).
48. F. Ramos, E. Dubois, A. Piérard, Control of enzyme synthesis in the lysine biosynthetic pathway of *Saccharomyces cerevisiae*. Evidence for a regulatory role of gene *LYS14*. *Eur. J. Biochem.* **171**, 171–176 (1988).
49. A. Feller, F. Ramos, A. Piérard, E. Dubois, In *Saccharomyces cerevisae*, feedback inhibition of homocitrate synthase isoenzymes by lysine modulates the activation of *LYS* gene expression by Lys14p. *Eur. J. Biochem.* **261**, 163–170 (1999).
50. L. Vécsei, L. Szalárdy, F. Fülöp, J. Toldi, Kynurenines in the CNS: Recent advances and new questions. *Nat. Rev. Drug Discov.* **12**, 64–82 (2013).
51. F. Giorgini, P. Guidetti, Q. Nguyen, S. C. Bennett, P. J. Muchowski, A genomic screen in yeast implicates kynurenine 3-monooxygenase as a therapeutic target for Huntington disease. *Nat. Genet.* **37**, 526–531 (2005).
52. L. Liu, P. Cundiff, G. Abel, Y. Wang, R. Faigle, H. Sakagami, M. Xu, Z. Xia, Extracellular signal-regulated kinase (ERK) 5 is necessary and sufficient to specify cortical neuronal fate. *Proc. Natl. Acad. Sci. U.S.A.* **103**, 9697–9702 (2006).
53. W. Wang, Y. W. Pan, J. Zou, T. Li, G. M. Abel, R. D. Palmiter, D. R. Storm, Z. Xia, Genetic activation of ERK5 MAP kinase enhances adult neurogenesis and extends hippocampus-dependent long-term memory. *J. Neurosci.* **34**, 2130–2147 (2014).
54. P. Daran-Lapujade, S. Rossell, W. M. van Gulik, M. A. H. Luttik, M. J. L. de Groot, M. Slijper, A. J. R. Heck, J. M. Daran, J. H. de Winde, H. V. Westerhoff, J. T. Pronk, B. M. Bakker, The fluxes through glycolytic enzymes in *Saccharomyces cerevisiae* are predominantly regulated at posttranscriptional levels. *Proc. Natl. Acad. Sci. U.S.A.* **104**, 15753–15758 (2007).
55. Z. Gu, L. M. Steinmetz, X. Gu, C. Scharfe, R. W. Davis, W. H. Li, Role of duplicate genes in genetic robustness against null mutations. *Nature* **421**, 63–66 (2003).
56. D. Fisher, L. Krasinska, D. Coudreuse, B. Novák, Phosphorylation network dynamics in the control of cell cycle transitions. *J. Cell Sci.* **125**, 4703–4711 (2012).
57. B. M. C. Martins, P. S. Swain, Ultrasensitivity in phosphorylation-dephosphorylation cycles with little substrate. *PLOS Comput. Biol.* **9**, e1003175 (2013).
58. G. G. Zampar, A. Kümmel, J. Ewald, S. Jol, B. Niebel, P. Picotti, R. Aebersold, U. Sauer, N. Zamboni, M. Heinemann, Temporal system-level organization of the switch from glycolytic to gluconeogenic operation in yeast. *Mol. Syst. Biol.* **9**, 651 (2013).
59. J. J. Villafranca, A. S. Mildvan, The mechanism of aconitase action. II. Magnetic resonance studies of the complexes of enzyme, manganese(II), iron(II) and substrates. *J. Biol. Chem.* **246**, 5791–5798 (1971).
60. J. D. Aguirre, V. C. Culotta, Battles with iron: Manganese in oxidative stress protection. *J. Biol. Chem.* **287**, 13541–13548 (2012).
61. A. D. Ogunniyi, L. K. Mahdi, M. P. Jennings, A. G. McEwan, C. A. McDevitt, M. B. V. der Hoek, C. J. Bagley, P. Hoffmann, K. A. Gould, J. C. Paton, Central role of manganese in regulation of stress responses, physiology, and metabolism in *Streptococcus pneumoniae*. *J. Bacteriol.* **192**, 4489–4497 (2010).
62. W. Zheng, S. Ren, J. H. Graziano, Manganese inhibits mitochondrial aconitase: A mechanism of manganese neurotoxicity. *Brain Res.* **799**, 334–342 (1998).
63. J. Y. Chen, G. C. Tsao, Q. Zhao, W. Zheng, Differential cytotoxicity of Mn(II) and Mn(III): Special reference to mitochondrial [Fe-S] containing enzymes. *Toxicol. Appl. Pharmacol.* **175**, 160–168 (2001).
64. D. R. Crooks, M. C. Ghosh, M. Braun-Sommargren, T. A. Rouault, D. R. Smith, Manganese targets m-aconitase and activates iron regulatory protein 2 in AF5 GABAergic cells. *J. Neurosci. Res.* **85**, 1797–1809 (2007).
65. K. Barnese, E. B. Gralla, J. S. Valentine, D. E. Cabelli, Biologically relevant mechanism for catalytic superoxide removal by simple manganese compounds. *Proc. Natl. Acad. Sci. U.S.A.* **109**, 6892–6897 (2012).
66. V. M. Anoop, U. Basu, M. T. McCammon, L. McAlister-Henn, G. J. Taylor, Modulation of citrate metabolism alters aluminum tolerance in yeast and transgenic canola overexpressing a mitochondrial citrate synthase. *Plant Physiol.* **132**, 2205–2217 (2003).
67. C. Verduyn, E. Postma, W. A. Scheffers, J. P. Van Dijken, Effect of benzoic acid on metabolic fluxes in yeasts: A continuous-culture study on the regulation of respiration and alcoholic fermentation. *Yeast* **8**, 501–517 (1992).
68. J. M. Cherry, E. L. Hong, C. Amundsen, R. Balakrishnan, G. Binkley, E. T. Chan, K. R. Christie, M. C. Costanzo, S. S. Dwight, S. R. Engel, D. G. Fisk, J. E. Hirschman, B. C. Hitz, K. Karra, C. J. Krieger, S. R. Miyasato, R. S. Nash, J. Park, M. S. Skrzypek, M. Simison, S. Weng, E. D. Wong, Saccharomyces Genome Database: The genomics resource of budding yeast. *Nucleic Acids Res.* **40**, D700–D705 (2012).
69. J. M. Buescher, S. Moco, U. Sauer, N. Zamboni, Ultrahigh performance liquid chromatography–tandem mass spectrometry method for fast and robust quantification of anionic and aromatic metabolites. *Anal. Chem.* **82**, 4403–4412 (2010).
70. J. D. Storey, A direct approach to false discovery rates. *J. R. Stat. Soc. Ser. B* **64**, 479–498 (2002).


**Acknowledgments:** We are grateful to C. Kraft for providing the single gene knockouts of kinases and phosphatases in *S. cerevisiae*, A. Chu and J. Horecka for providing the prototrophic *ppq1*Δ strain, D. C. Thomas for constructing the $Lys^{20}$ and $Lys^{21}$ plasmids, and L. Falter for her assistance in experiment design. **Funding:** This work was supported by the SystemsX.ch project YeastX and by an ETH postdoctoral fellowship to M.Z. **Author contributions:** M.Z., J.C.S., and U.S. prepared and edited the manuscript. J.C.S. performed the nontargeted metabolomics screen, the follow-up experiments, and the statistical data analysis. M.Z. devised and implemented the locality scoring statistical analysis, and performed follow-up experiments and statistical analysis. S.W. and C.v.M. analyzed the data. **Data and materials availability:** Raw MS data are available upon request.

Submitted 18 June 2014
Accepted 5 November 2014
Final Publication 25 November 2014
10.1126/scisignal.2005602
**Citation:** J. C. Schulz, M. Zampieri, S. Wanka, C. von Mering, U. Sauer, Large-scale functional analysis of the roles of phosphorylation in yeast metabolic pathways. *Sci. Signal.* **7**, rs6 (2014).

**Large-scale functional analysis of the roles of phosphorylation in yeast metabolic pathways**

Juliane Caroline Schulz, Mattia Zampieri, Stefanie Wanka, Christian von Mering and Uwe Sauer (November 25, 2014)

*Science Signaling* **7** (353), rs6. [doi: 10.1126/scisignal.2005602]